Effect of Combined Addition of Cu and Aluminum Oxide Nanoparticles on Mechanical Properties and Microstructure of Al-7Si-0.3Mg Alloy

HONGSEOK CHOI, MILTON JONES, HIROMI KONISHI, and XIAOCHUN LI

In this study, an ultrasonic cavitation based dispersion technique was used to fabricate Al-7Si-0.3Mg alloyed with Cu and reinforced with 1 wt pct Al_2O_3 nanoparticles, in order to investigate their influence on the mechanical properties and microstructures of Al-7Si-0.3Mg alloy. The combined addition of 0.5 pct Cu with 1 pct Al_2O_3 nanoparticles increased the yield strength, tensile strength, and ductility of the as-cast Al-7Si-0.3Mg alloy, mostly due to grain refinement and modification of the eutectic Si and θ-CuAl$_2$ phases. Moreover, Al-7Si-0.3Mg-0.5Cu-1 pct Al_2O_3 nanocomposites after T6 heat treatment showed a significant enhancement of ductility (increased by 512 pct) and tensile strength (by 22 pct). The significant enhancement of properties is attributed to the suppression of pore formation and modification of eutectic Si phases due to the addition of Al_2O_3 nanoparticles. However, the yield strength of the T6 heat-treated nanocomposites was limited in enhancement due to a reaction between Mg and Al_2O_3 nanoparticles.

I. INTRODUCTION

ALUMINUM-SILICON (Al-Si) alloys compromise 85 to 90 pct of the total Al casting parts produced commercially, and are used extensively in industry due to their superior properties, including good corrosion resistance, low coefficient of thermal expansion, excellent castability, low density, high strength-to-weight ratio, and improved mechanical properties over a wide range of temperatures.[1] Especially, as-cast A356 alloy, a hypoeutectic Al-7Si-0.3Mg alloy, is widely used in the automobile and aerospace industries because of its good strength and ductility, compared to other Al alloys. In addition, heat-treated A356 alloy exhibits even higher performance, including much improved ductility, pressure tightness, and corrosion resistance.[2] Even though A356 exhibits good performance in as-cast as well as in its heat-treated form, the alloy has several limitations. For example, A356 exhibits moderate machinability, low stiffness, and limited strength under high temperatures, which limits its application to components subjected to extreme temperature conditions.[3] In addition, A356 exhibits low room temperature wear resistance as well as the presence of defects and oxide films.[4] Therefore, there have been many studies to further improve the mechanical performance of A356 alloy

through additional element alloying or reinforcements for the expanded applications in industry.

Addition of Cu in Al-Si-Mg alloy has been reported to increase its hardness by 4.5 pct[5] and enhance its ultimate tensile strength up to 6 pct.[6] Although Cu alloying has a positive effect on strengthening Al-Si or Al-Si-Mg alloys, there are some drawbacks as well. For example, Cu addition leads to a significant increase in porosity, which results in a deterioration of ductility, corrosion and hot-tearing resistance, and castability. Caceres et al. reported that the porosity of Al-Si-Mg alloy with 0.5 wt pct Cu increased 4 times as high as that of Al-Si-Mg alloy without additional Cu element.[7]

Metal matrix nanocomposites (MMNCs) with ceramic nanoparticle reinforcements have been studied recently because of their potential to strengthen the Al matrix, while maintaining or even enhancing ductility.[8,9] However, most processing techniques for MMNCs are not capable of producing bulk nanocomposite casting of complex shapes. It is also extremely difficult to uniformly disperse nanoparticles in metal melts due to their high specific surface areas, which easily induce agglomeration and clustering.[10] Recently, a novel technique, ultrasonic-cavitation based solidification processing, was developed to disperse and distribute nanoparticles in metal melts.[10–12] Magnesium and Al MMNCs were successfully fabricated. Experimental results show a nearly uniform distribution and good dispersion of the SiC nanoparticles in the metal matrix by ultrasonic cavitation, resulting in significantly enhanced mechanical strength while maintaining or improving ductility. The micro hot spots with temperatures of about 5273 K (5000 °C), pressures above 1000 atm, and heating and cooling rates above 1283 K/s can be produced by the ultrasonic cavita-

HONGSEOK CHOI and HIROMI KONISHI, Assistant Scientists, and XIAOCHUN LI, Professor, are with the Department of Mechanical Engineering, University of Wisconsin-Madison, Madison, WI 53706. Contact e-mail: xcli@engr.wisc.edu MILTON JONES, formerly Graduate Research Assistant with the Materials Science Program, University of Wisconsin-Madison, is now R&D Process Engineer with the Brady Corporation, Milwaukee, WI 53201-0571.
Manuscript submitted October 1, 2010.
Article published online September 16, 2011

tion.[13] The transient, localized implosive impact induced by the ultrasonic cavitation can effectively disperse nanoparticles in metal melts.

Among various kinds of ceramic particles such as oxides, nitrides, or carbides, Al_2O_3 is widely used as reinforcement particles due to its relatively good thermal and chemical stability as compared to other types of reinforcements.[14,15] This article illustrates the effect of the combined addition of Cu and ultrasonically dispersed Al_2O_3 nanoparticles on the microstructure and overall mechanical properties of as-cast and heat-treated Al-7Si-0.3Mg alloy.

II. MATERIALS AND EXPERIMENTAL PROCEDURE

A. Selection of Reinforcement Nanoparticles

In this study, γ-Al_2O_3 nanoparticles (99.97 pct purity, Nanostructured & Amorphous Materials, Inc., Houston, TX) with a diameter of 25 nm were used as the reinforcing material for strengthening of Al-7Si-0.3Mg alloy. The γ-Al_2O_3 nanoparticles were selected due to higher catalytic potencies in nucleating the α-Al phase of hypoeutectic Al-Si alloy, compared with α-Al_2O_3 nanoparticles.[16] The γ-Al_2O_3 nanoparticle has a density of 3.7 g/cm^3 and a specific surface area of 180 m^2/g.

B. Experimental Setup

Figure 1 illustrates a schematic of the experimental setup for the ultrasonic-cavitation based dispersion processing of Al_2O_3 nanoparticles for Al-7Si-0.3Mg-Cu nanocomposites. The system consists of a resistance heating furnace, a protection gas system, a nanoparticle feeding system, and an ultrasonic processing system. The graphite crucible with a diameter of 38.1 mm and a height of 76.2 mm was used for melting, ultrasonic processing, and casting. The ultrasonic processing system consists of an ultrasonic probe, booster, and transducer. A niobium ultrasonic probe with a diameter
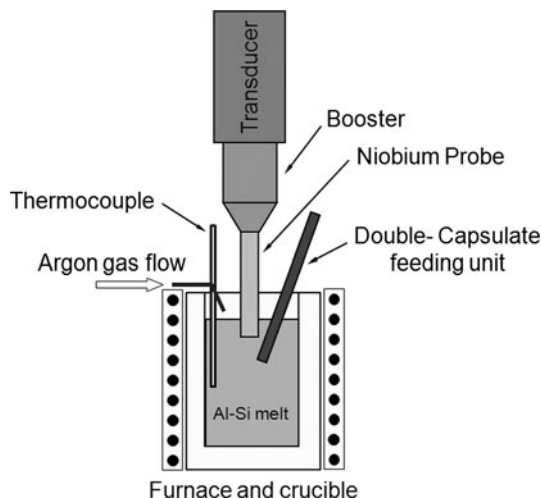

Fig. 1—Schematics of experimental setup for ultrasonic processing.

of 12.7 mm and a length of 92 mm was attached to a booster (Sonicator 3000, Misonix Inc., Farmingdale, NY), which was mounted in a transducer working under a frequency of 20 kHz and a maximum 600 W power output. A double-capsulate feeding method was used to feed γ-Al_2O_3 nanoparticles into the melt. In the double-capsulate feeding method, nanoparticles were wrapped with 0.0127-mm thin Al foil (alloy 1000), and then the Al foil was rolled into a rod shape with a diameter of about 6 mm (making the first capsule). The Al foil rod, entrapping the nanoparticles, was wrapped again with another thin Al foil (alloy 1100) with a dimension of 355.6 mm × 152.4 mm and a thickness of 0.0254 mm (making the second capsule). The second Al foil would make the nanoparticles discharge into the melt gradually, resulting from the gradual melting of the thicker wall of the capsule. In order to avoid oxidation of the Al melt, all processes were protected with Ar gas, which was injected at a constant flow rate through two gas nozzles.

C. Nanoparticles Feeding and Casting

Al-Si melts were prepared to develop a material with a composition of 7 wt pct Si, 0.3 wt pct Mg, and the remaining balance of Al, in order to model the composition of the A356 alloy, without the presence of negligible elements present in A356 ingots (Mn, Fe, Zn, Ni, Ti). Pure Al (99.8 pct) ingots and pure Mg (99.93 pct) stock additions were used for alloying, and Si was alloyed into the melt through the addition of a binary Al-Si (50 wt pct Si) master alloy. 0.5 wt pct, 0.75 wt pct, and 1 wt pct Cu was alloyed in the melt using a Cu 110 alloy foil, 0.2 mm in thickness. About 160 g of Al alloy was melted in the graphite crucible under protective argon gas. The Al-Si-Mg-Cu melt was degassed, using a N_2 + 1 pct Cl_2 gas, for 2 minutes at 1013 K (740 °C). After that, the tip of the niobium ultrasonic probe was inserted about 12.7 mm in depth into the melt of 973 K (700 °C). Ultrasonic vibration with a frequency of 20 kHz and a peak-to-peak amplitude of 60 μm was generated from the transducer, and then preheated γ-Al_2O_3 nanoparticles [423 K (150 °C) for 1 hour] were added into the melt with the double-capsulate feeding method during ultrasonic processing. One Al foil capsule with a total weight of 4.6 g (containing γ-Al_2O_3 nanoparticles) was slowly fed into the melt and ultrasonically processed within the melt. The melt was ultrasonically processed for 15 minutes for each Al foil capsule, bringing a total processing time of 45 minutes. After the ultrasonic processing for 45 minutes, the ultrasonic probe was lifted out of the melt and the temperature of the melt was increased to 1013 K (740 °C) for pouring. The melt was cast into a low carbon steel permanent mold preheated to 623 K (350 °C). Two standard flat tensile specimens with a gage dimension of 6.35 mm × 6.35 mm and a gage length of 38.1 mm were obtained after each casting.

D. Heat Treatment Procedure

T6 heat treatment was performed according to ASTM standard E466. The tensile specimens of pure alloy and

its Al_2O_3 nanocomposite were heat treated inside a box furnace (Blue M Model 51333, Lindberg, Asheville, NC) preheated to 813 K ± 6 K (540 °C ± 6 °C) for solution treatment for 12 hours. At the end of solution treatment, the tensile specimens were immediately submerged into a water bath and heated at 355 K (82 °C) for quenching for 1 minute. After quenching, the tensile specimens were air cooled and then repositioned inside the furnace preheated at the aging temperature of 428 K ± 6 K (155 °C ± 6 °C) for 4 hours. After the aging process was finished, the tensile specimens were cooled at air.

E. Mechanical Characterization

Mechanical properties of as-cast and T6 heat-treated alloys were determined using a tensile testing machine (Sintech 10/GL, MTS Systems Corp., Eden Prairie, MN) with a crosshead speed of 5.08 mm/min. An extensometer with a 25.4-mm gage length was employed for an accurate measurement of yield strength. The crosshead speed was set to 5.08 mm/min. When the strain reached 0.2 pct, the tensile testing machine paused temporarily so that the extensometer could be removed. Final ductility was measured manually after putting the two tested sample pieces back together according to ASTM B 557-06.

F. Microstructural Characterization

For microstructural characterization, polished samples were lightly etched using a 0.5 pct HF-water etchant. Optical micrographs were taken of the samples to study their overall microstructure and to measure grain size through the linear intercept method, as described by ASTM standard E112, as well as to measure dendrite arm spacing (DAS), described by SAE ARP standard 1947. Scanning electron microscopy (SEM, Leo 1530, Carl Zeiss SMT, Inc., Peabody, MA) and scanning transmission electron microscopy (STEM, Titan-80-200, FEI, Hilsboro, OR) were also used for detailed metallographic analysis.

III. EXPERIMENTAL RESULTS AND DISCUSSION

A. As-Cast Al-7Si-0.3Mg-Cu Alloys and Nanocomposites

The average 0.2 pct yield strength, ultimate tensile strength, and ductility of as-cast pure Al-7Si-0.3Mg alloys with varying content of Cu (0.5, 0.75, and 1 wt pct) are shown in Table I. It is seen from Table I that the alloying of Cu, in various percentages, helps to strengthen the Al-7Si-0.3Mg matrix. This result is in agreement with the previously reported experimental results[5,6] that the addition to Cu improves the mechanical strength of the Al-Si-Mg alloys through the formation of the hardened θ-CuAl$_2$ phases. This hardened θ phase prefers to nucleate on eutectic Si particles. However, even though Cu alloying contributes to enhancing the strength of the Al-7Si-0.3Mg alloy, Cu also limits the alloy's enhancement in ductility, as shown in Table I. The limits in ductility, as a result of Cu additions, is expected, as Caceres et al.[7] concluded that the Cu alloying in Al-Si alloys limits or decreases the alloy's ductility. This limitation of ductility is, in part, due to the large solidification interval (for example, 378 K (105 °C) in alloy Al-6Si-3.5Cu[7]) for the θ-CuAl$_2$ phases, which leads to increased porosity and defects.

In Table I, it is also observed that the Al-7Si-0.3Mg-0.5Cu-1 pct Al_2O_3 nanocomposite shows the largest enhancement of 0.2 pct yield strength (13 pct), ultimate tensile strength (33 pct), and ductility (163 pct), of the three different Cu contents, compared with its pure alloy. Therefore, it is determined that 0.5 wt pct Cu along with the reinforcement of 1 wt pct Al_2O_3 particles would be appropriate to achieve good strength and ductility. This selected Cu content is not the optimal content of Cu for the pure alloys to offer optimal strength or ductility. The addition of 1 wt pct Cu to Al-7Si-0.3Mg alloy shows the maximum enhancement in mechanical properties in the tested range of Cu additions (0 to 1.0 wt pct). The addition of Cu improves the mechanical strength of the Al-7Si-0.3Mg alloy or A356 alloy, caused by the nucleation of hardened θ-CuAl$_2$ phases. However, the θ-CuAl$_2$ phases deteriorate the ductility of alloys due to their large solidification interval, which leads to the increase of probability of porosity generation.[17] It is worth noting that Al-7Si-0.3Mg-0.5Cu-1 pct Al_2O_3 nanocomposite shows significant enhancements in ductility and strength. For Al-7Si-0.3Mg-0.5Cu-1 pct Al_2O_3 nanocomposite, the ductility is improved from 3 to 7.9 pct (increased by 163 pct). This implies that the combination of Cu and γ-Al_2O_3 nanoparticles produces beneficial effects on the mechanical properties, especially ductility of Al-7Si-0.3Mg alloy.

Optical micrographs and SEM photographs of the as-cast pure Al-7Si-0.3Mg-0.5Cu alloy and its nanocomposites are shown in Figure 2. As shown in Figure 2(a),

Table I.   Mechanical Properties of As-Cast Al-7Si-0.3Mg-Cu Alloys and their Nanocomposites

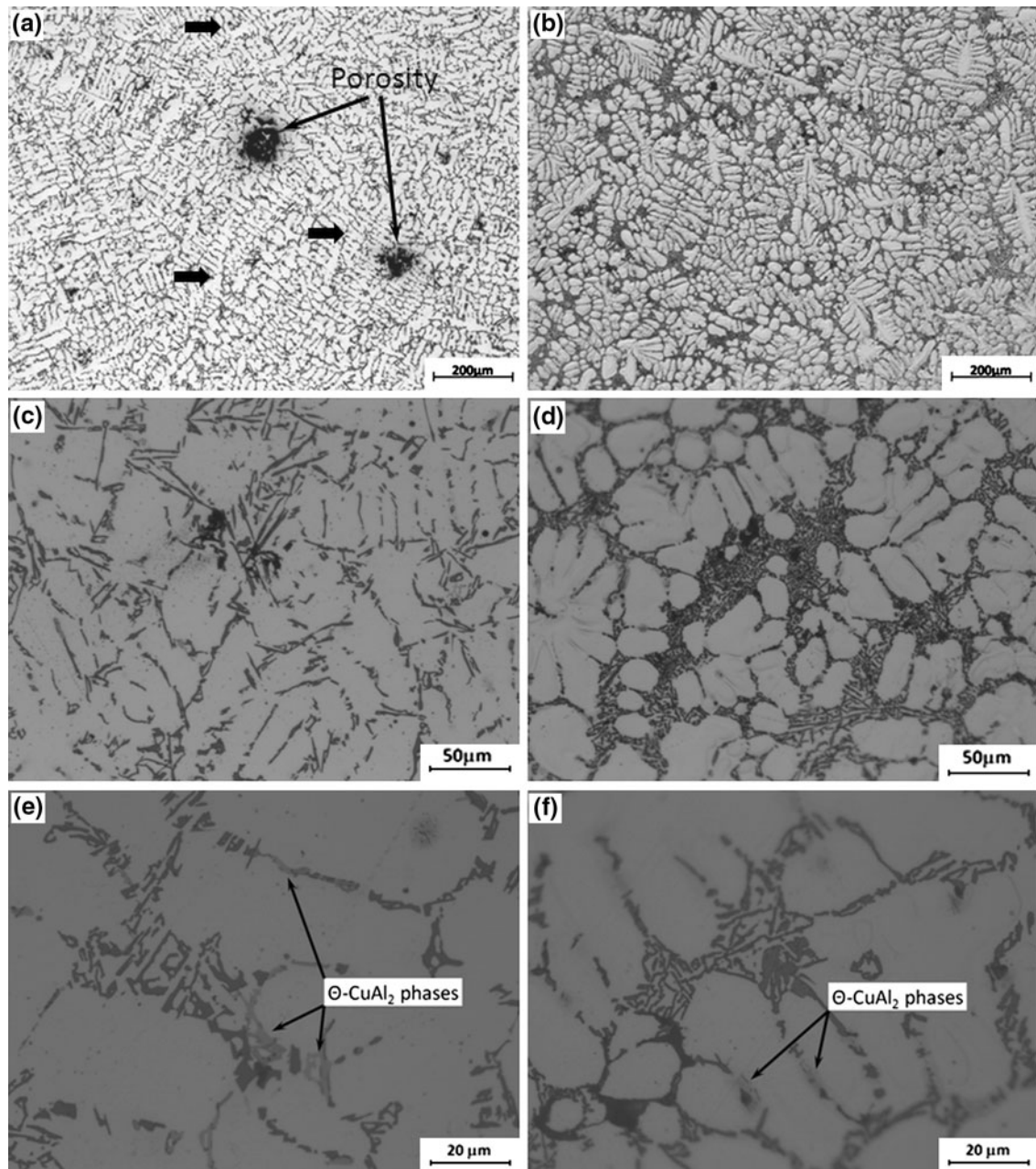| Alloys and Nanocomposites	Yield Strength (MPa)	Ultimate Tensile Strength (MPa)	Ductility (Pct)
Pure Al-7Si-0.3Mg-0.5Cu	97.0 ± 4	148.5 ± 2	3.0 ± 0.1
Al-7Si-0.3Mg-0.5Cu-1Al$_2$O$_3$	110.0 ± 3	197.5 ± 6	7.9 ± 0.6
Pure Al-7Si-0.3Mg-0.75Cu	103.0 ± 2	170.0 ± 10	4.4 ± 2
Al-7Si-0.3Mg-0.75Cu-1Al$_2$O$_3$	107.5 ± 4	190.5 ± 10	6.5 ± 0.8
Pure Al-7Si-0.3Mg-1.0Cu	112.5 ± 1	177.5 ± 8	3.7 ± 0.5
Al-7Si-0.3Mg-1.0Cu-1Al$_2$O$_3$	110.0 ± 5	195.5 ± 10	5.6 ± 1
Pure Al-7Si-0.3Mg	94 ± 0	153 ± 10	4.7 ± 0.7

Fig. 2—Optical micrographs of Al-7Si-0.3Mg-0.5Cu alloy modified with (*a*), (*c*), and (*e*) 0 pct Al$_2$O$_3$ nanoparticles and (*b*), (*d*), and (*f*) 1 pct Al$_2$O$_3$ nanoparticles.

there are several large porosities in the as-cast pure Al-7Si-0.3Mg-0.5Cu alloy, which is induced by the addition of Cu. Figure 2(b), however, shows the presence of much less and smaller porosity within the matrix. The porosity was measured from the density deviation derived from theoretical and experimental values based on the Archimedes principle. An electronic balance with an accuracy of ±0.001 g was used for weighing samples. The density was calculated and compared to the theoretical rule-of-mixtures density. The resulting densities are shown in Table II with the calculated volume fractions of porosity. To make a more relevant comparison, the densities of all samples

were measured and then the volume fraction of porosity for each sample was calculated.

When the Cu content of Al-7Si-0.3Mg alloy increases from 0.5 pct, to 0.75 pct, and then to 1 pct, the porosity of the alloy is 2.3, to 3.1, and then to 3.3 pct, respectively. The porosity of the corresponding nanocomposites also becomes higher with a higher Cu content. However, all nanocomposites still show much reduced porosity (by about 70 pct) than that of their pure alloy counterparts. Therefore, this suggests that γ-Al$_2$O$_3$ nanoparticles are effective for the suppression of the growth of pores in Al-7Si-0.3Mg alloys with Cu addition. This limitation of pore growth results in the

Table II. Density and Porosity of As-Cast Al-7Si-0.3Mg-Cu Alloy and its Nanocomposite

Alloys and nanocomposites	Theoretical (g/cm^3)	Experimental (g/cm^3)	Porosity (Pct)
Pure Al-7Si-0.3Mg-0.5Cu	2.675	2.615 ± 0.004	2.3
Al-7Si-0.3Mg-0.5Cu-1Al$_2$O$_3$	2.682	2.666 ± 0.021	0.6
Pure Al-7Si-0.3Mg-0.75Cu	2.680	2.596 ± 0.012	3.1
Al-7Si-0.3Mg-0.75Cu-1Al$_2$O$_3$	2.687	2.664 ± 0.022	0.9
Pure Al-7Si-0.3Mg-1.0Cu	2.684	2.596 ± 0.009	3.3
Al-7Si-0.3Mg-1.0Cu-1Al$_2$O$_3$	2.692	2.653 ± 0.010	1.5
Pure Al-7Si-0.3Mg	2.666	2.654 ± 0.004	0.4

increase of ductility, while maintaining high strengthening achieved through Cu addition. Figure 2(a) shows coarse acicular eutectic Si phases dispersed among the fully developed primary α-Al dendrites (marked by arrows). In the middle of Figure 2(a), one dendrite arm is about 280 μm in length, which indicated that the grain size is about a few millimeters as one equiaxed grain usually contained several branches. In contrast, the Al-7Si-0.3Mg-0.5Cu Al$_2$O$_3$ nanocomposite reveals finer primary α-Al dendrites interspersed with a continuous phase of very fine eutectic Si (Figure 2(b)). The average DAS values of as-cast pure Al-7Si-0.3Mg-0.5Cu alloy and its Al$_2$O$_3$ nanocomposite are 20 and 12.5 μm, respectively (decreased by 37.5 pct). Refinement of primary α-Al dendrites would lead to enhancement of yield strength due to a limited dislocation motion and a slower fracture rate.

Figures 2(c) and (d) show that the shape and size of the eutectic Si phases in Al-7Si-0.3Mg-0.5Cu-1 pct Al$_2$O$_3$ nanocomposites are much smaller than those of pure Al-7Si-0.3Mg-0.5Cu alloy (decreased by 59 pct in length and 52 pct in width). Typical coarse acicular eutectic Si and large primary α-Al dendrites are observed in the pure Al-7Si-0.3Mg-0.5Cu alloy. In the case of nanocomposite, some fine eutectic Si phases are shown in Figure 2(d). The eutectic phase is flakelike, much thinner and shorter than that in the pure Al-7Si-0.3Mg-0.5Cu alloy. The size of individual eutectic phase is noticeably reduced as compared with that of the pure alloy. This might be attributed to a decrease in the probability of Si atoms to attach them on the growing eutectic Si phases, resulting from enhanced nucleation of eutectic phases caused by the added Al$_2$O$_3$ nanoparticles. Another interesting feature observed is that a lamellar spacing of eutectic phase is much smaller in the nanocomposite than the one in the pure alloy. The average lamellar spacing of eutectic phase was reduced from 5.8 ± 0.3 μm to 1.9 ± 0.4 μm. This might be a reason that the formed eutectic lamellae could not grow ahead due to the enhanced nucleation of eutectic phases. As a result, the eutectic lamellar spacing reduces by 67 pct.

Optical micrographs of θ-CuAl$_2$ phases in the as-cast pure Al-7Si-0.3Mg-0.5Cu alloy and its Al$_2$O$_3$ nanocomposite are shown in Figures 2(e) and (f). Although the θ-CuAl$_2$ phases in Al$_2$O$_3$ nanocomposite show similar size as that in pure Al-7Si-0.3Mg-0.5Cu alloy, the shape is modified from long platelets or lamellae into blocky or polygonal phases. It has been reported that the θ-CuAl$_2$ phases prefer to nucleate on eutectic Si phases and are solidified at the last stage of the solidification process of Al-Si-Mg-Cu alloys.[18,19] Therefore, the modification of the shape of θ-CuAl$_2$ phase in Al$_2$O$_3$ nanocomposite is attributed to the restraint of the nucleation and growth process of θ-CuAl$_2$ phases by neighboring refined fibrous eutectic Si. The modification of brittle θ-CuAl$_2$ phases is also partly related to the enhancement of nanocomposites in strength and ductility. Figure 3 shows SEM photographs of the θ-CuAl$_2$ phases in the as-cast pure Al-7Si-0.3Mg-0.5Cu alloy and its Al$_2$O$_3$ nanocomposite. EDS spectrum spot analysis in SEM revealed the peaks of Al and Cu, indicating the presence of θ-CuAl$_2$ phases in Al-7Si-0.3Mg-0.5Cu-1 wt pct Al$_2$O$_3$ nanocomposite (Figure 3(c)). Moreover, STEM analysis and electronic diffraction (ED) comparison were used to confirm the phase. The result revealed that the ED pattern matched that of θ-CuAl$_2$, as shown in Figure 3(d).

In Figure 4(a), the STEM photograph shows that Al$_2$O$_3$ nanoparticle microclusters (marked by white arrows) are distributed around the edges and tips of eutectic Si phases (indicated by black arrows) in the Al matrix. The ED pattern in those areas matched with that of γ-Al$_2$O$_3$. It is likely that the γ-Al$_2$O$_3$ nanoparticles adjacent to eutectic Si phases could restrict the growth of eutectic Si and partly modify its morphology. While some nanoparticles still appear as microclusters in Figure 4(a), these microclusters are still separated to single nanoparticles or small agglomerated nanoclusters. As shown in Figure 4(b), the γ-Al$_2$O$_3$ nanoparticles have a random orientation in the Al-7Si-0.3Mg-0.5Cu-1 wt pct Al$_2$O$_3$ nanocomposite matrix. Moreover, Moire fringes of γ-Al$_2$O$_3$ nanoparticles can be observed, indicating no intermediate phase between the γ-Al$_2$O$_3$ nanoparticle and the matrix. The γ-Al$_2$O$_3$ nanoparticles have a high potency for catalysis of nucleation of α-Al phases in hypoeutectic Al-Si alloy.[16] The γ-Al$_2$O$_3$ has a cubic structure with $a = 7.9$ Å,[20] and Al also has a faceted cubic crystal with a lattice constant $a = 4.05$ Å.[21] Since the lattice constant of γ-Al$_2$O$_3$ is about 2 times as large as that of Al, a good compatibility of the crystal structure between Al and γ-Al$_2$O$_3$ nanoparticle could exist. The lattice mismatch of γ-Al$_2$O$_3$ with Al is only 2.5 pct, as 4.05 Å $\times$ 2 = 8.1 Å, making γ-Al$_2$O$_3$ potent act as the heterogeneous nucleus of the α-Al phase during solidification. In the case with Si (lattice constant $a = 5.4$ Å[22]), the lattice mismatch of γ-Al$_2$O$_3$ is about 3 pct, as 5.4 Å $\times \sqrt{2}$ = 7.64 Å. Therefore, this suggests that γ-Al$_2$O$_3$ nanoparticles could be a suitable nucleant of α-Al phase and a modifying agent of eutectic Si during the solidification of Al-7Si-0.3Mg-0.5Cu alloy.
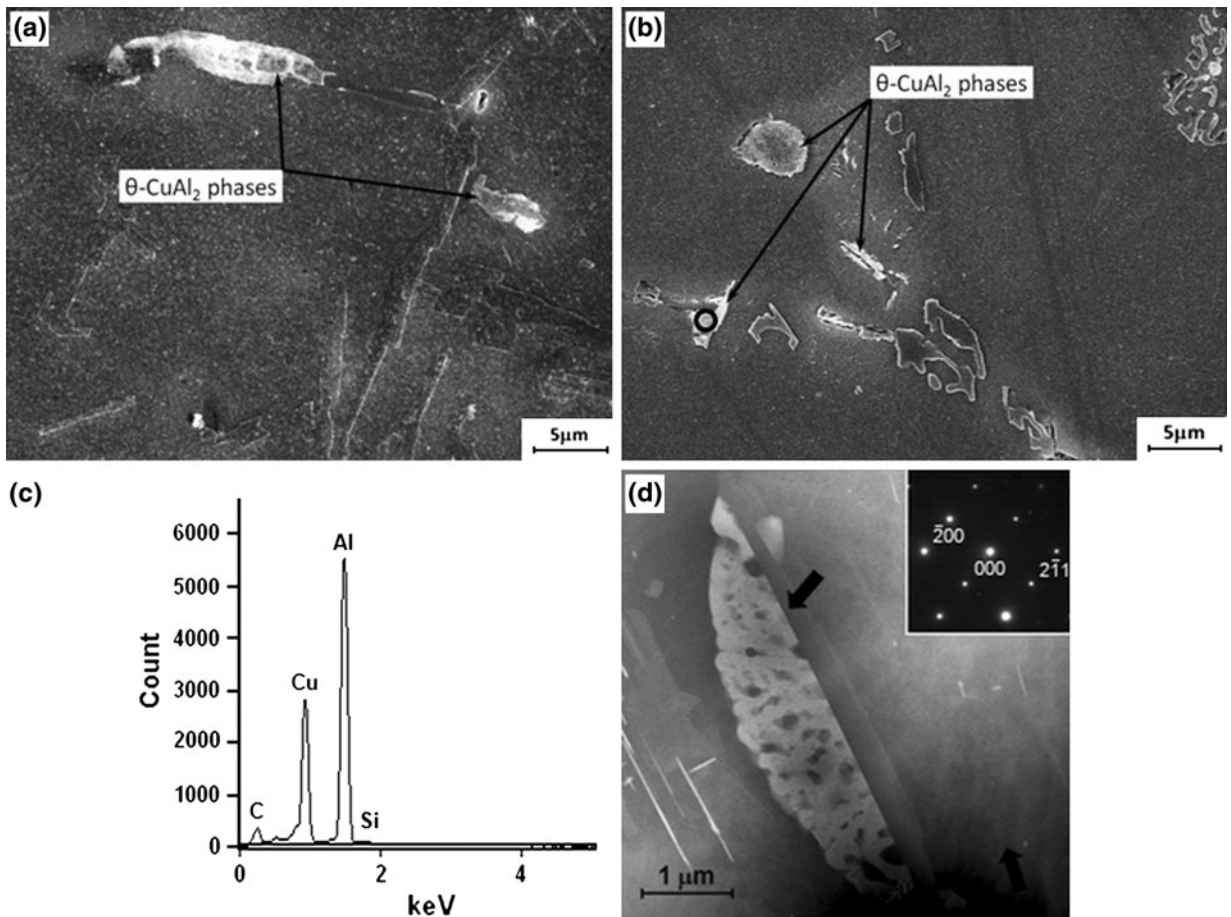
Fig. 3—SEM photographs of Al-7Si-0.3Mg-0.5Cu alloy modified with (a) 0 pct Al_2O_3 nanoparticles, (b) 1 pct Al_2O_3 nanoparticles, (c) spot EDS spectrum (indicated by the circle in b), and (d) TEM photograph and electron diffraction pattern of θ-$CuAl_2$ (marked by arrow) in Al-7Si-0.3Mg-0.5Cu-1 pct Al_2O_3 nanocomposite.
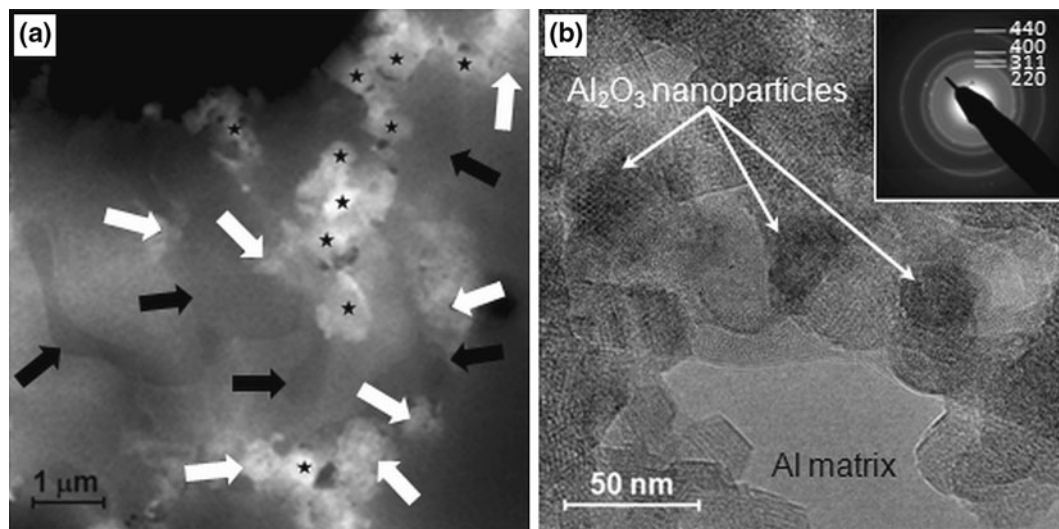

Fig. 4—(a) TEM photograph of eutectic Si phases (indicated by black arrows), Al_2O_3 nanoparticles clusters (marked by white arrows), and $MgAl_2O_4$ spinels (marked with black stars) in Al-7Si-0.3Mg-0.5Cu-1 pct Al_2O_3 nanocomposite. (b) TEM photograph and electron diffraction pattern of Al_2O_3 nanoparticle.

B. T6 Heat-Treated Al-7Si-0.3Mg-Cu Alloy and Nanocomposite

The mechanical properties of T6 heat-treated pure Al-7Si-0.3Mg-0.5Cu alloy and its 1 wt pct Al_2O_3 nanocomposite are shown in Table III. From Table III, it is seen that T6 heat-treated pure Al-7Si-0.3Mg-0.5Cu alloy exhibits enhancements in strength (by 103 pct in yield strength and by 64 pct in ultimate tensile strength) compared with that of the as-cast pure alloy. It has been reported that the addition of Cu into Al-Si-Mg alloys enhances the precipitation hardening kinetics of Al-Si-Mg alloys, resulting in improved strength.[23] However, the ductility of T6 heat-treated pure Al-7Si-0.3Mg-0.5Cu alloy decreases by 43 pct compared with that of as-cast pure alloy. Caceres et al.[7] reported that Cu-rich, heat-treated Al-Si-Mg alloys have undissolved θ-$CuAl_2$ phases due to a restricted solution temperature, resulting in an increase of the probability of porosity formation and lower ductility.

In addition, it is clearly shown in Table III that the T6 heat-treated nanocomposite has a significant enhancement in ultimate tensile strength (22 pct) and ductility (512 pct) than T6 heat-treated pure Al-7Si-0.3Mg-0.5Cu. The ductility is increased from 1.7 to 10.4 pct. Figure 5 shows optical micrographs and SEM photographs of the T6 heat-treated pure Al-7Si-0.3Mg-0.5Cu alloy and its Al_2O_3 nanocomposite. T6 heat-treated pure Al-7Si-0.3Mg-0.5Cu alloy (Figure 5(a)) shows the presence of pores, which is consistent with the microstructure observation of as-cast pure Al-7Si-0.3Mg-0.5Cu alloy. However, the formation of porosity is suppressed with the addition of Al_2O_3 nanoparticles, as shown in Figure 5(b). Table IV shows that the porosity of T6 heat-treated Al-7Si-0.3Mg-0.5Cu-1 wt pct Al_2O_3 nanocomposite is about 79 pct lower than that of T6 heat-treated pure Al-7Si-0.3Mg-0.5Cu alloy. The reduction of porosity is similar to the case of as-cast alloy and its Al_2O_3 nanocomposite. Moreover, it can be seen that a

Table III. Mechanical Properties of T6 Heat-Treated Pure Al-7Si-0.3Mg-0.5Cu Alloy and its Al₂O₃ Nanocomposite

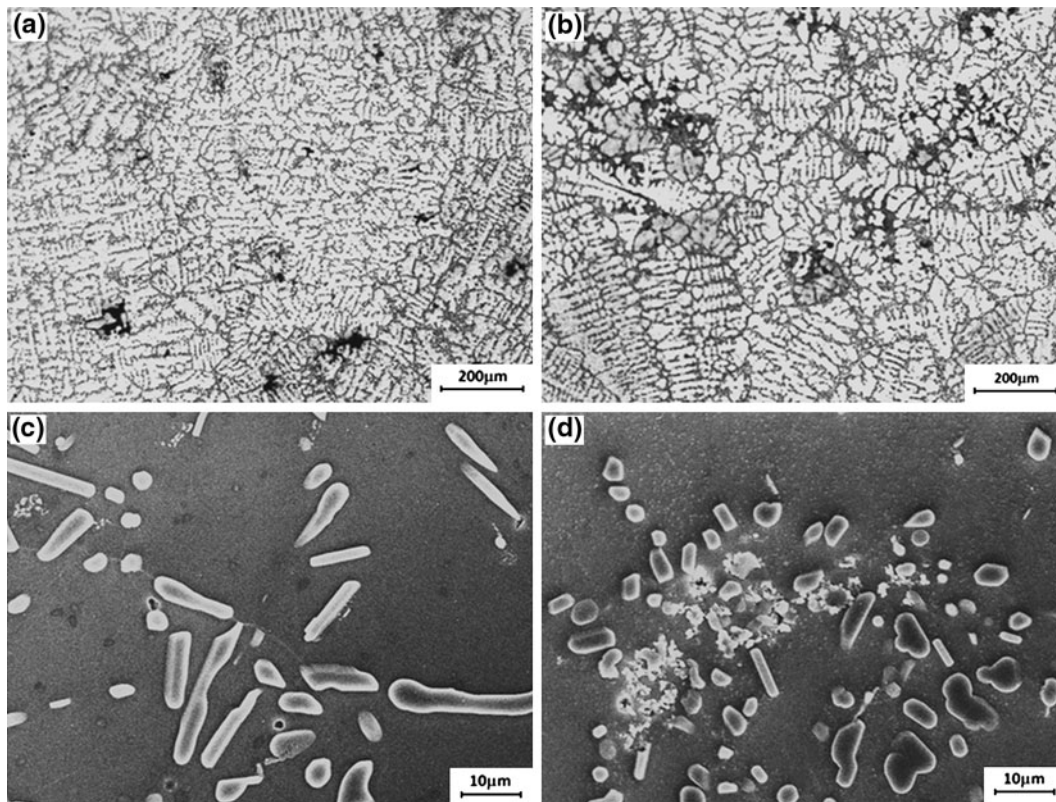| Alloys and Nanocomposites	Yield Strength (MPa)	Ultimate Tensile Strength (MPa)	Ductility (Pct)
Pure Al-7Si-0.3Mg-0.5Cu, T6	197.0 ± 7	243.0 ± 3	1.7 ± 0.2
Al-7Si-0.3Mg-0.5Cu-1Al₂O₃, T6	195.0 ± 2	297.5 ± 10	10.4 ± 4
Pure Al-7Si-0.3Mg, T6	167 ± 0.5	256 ± 0	7.45 ± 0.2

Fig. 5—Optical micrographs and SEM photographs of T6 heat-treated Al-7Si-0.3Mg-0.5Cu alloys modified with (a) and (c) 0 pct Al_2O_3 nanoparticles and (b) and (d) 1 pct Al_2O_3 nanoparticles.

Table IV. Density and Porosity of T6 Heat-Treated Al-7Si-0.3Mg-Cu Alloy and its Nanocomposite

Alloys and Nanocomposites	Theoretical (g/cm³)	Experimental (g/cm³)	Porosity (Pct)
Pure Al-7Si-0.3Mg-0.5Cu, T6	2.675	2.611 ± 0.005	2.4
Al-7Si-0.3Mg-0.5Cu-1Al₂O₃, T6	2.684	2.668 ± 0.018	0.5
Pure Al-7Si-0.3Mg, T6	2.666	2.657 ± 0.002	0.3
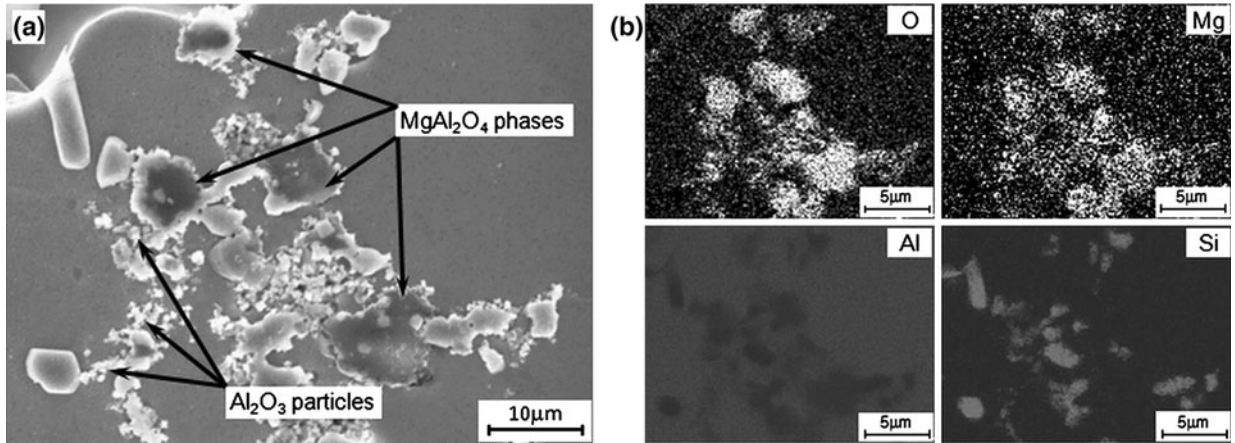
Fig. 6—SEM photograph and EDS spectral mapping of T6 heat-treated Al-7Si-0.3Mg-0.5Cu-1 pct Al_2O_3 nanocomposite.

slight refinement of primary α-Al grain occurs in the nanocomposites. The average grain size of T6 heat-treated pure Al-7Si-0.3Mg-0.5Cu alloy and its Al_2O_3 nanocomposite are 120 and 115 μm, respectively.

SEM photographs of the eutectic Si phases in T6 heat-treated pure Al-7Si-0.3Mg-0.5Cu alloy and its Al_2O_3 nanocomposites are shown in Figures 5(c) and (d). The eutectic Si phases in T6 heat-treated Al-7Si-0.3Mg-0.5Cu-1 wt pct Al_2O_3 nanocomposite (Figure 5(d)) are smaller in size and shape than those in T6 heat-treated pure Al-7Si-0.3Mg-0.5Cu alloy (Figure 5(c)). The average length of eutectic Si phases was decreased by 49 pct, while their width was slightly reduced (by 9 pct) in T6 heat-treated Al-7Si-0.3Mg-0.5Cu-1 wt pct Al_2O_3 nanocomposite. This is possibly due to the fact that, even though the T6 heat treatment process refines the eutectic Si phases, the nucleation of eutectic Si is enhanced with the addition of γ-Al_2O_3 nanoparticles, such as the case of as-cast Al_2O_3 nanocomposite, resulting in rounder and smaller eutectic Si phases than those in the T6 heat-treated pure Al-7Si-0.3Mg-0.5Cu alloy. The refinement of eutectic Si phases due to the addition of Al_2O_3 nanoparticles limits the initiation of cracks, which can easily happen on coarse acicular eutectic Si phases.[24] This limitation of crack initiation at the interface between primary α-Al and eutectic Si can be partly attributed to the enhancement in tensile strength and ductility of T6 heat-treated Al-7Si-0.3Mg-0.5Cu-1 wt pct Al_2O_3 nanocomposite.

Although the ultimate tensile strength and ductility are significantly enhanced with the addition of Al_2O_3 nanoparticles into the T6 heat-treated Al-7Si-0.3Mg-0.5Cu alloy, Table III shows that the T6 heat-treated Al-7Si-0.3Mg-0.5Cu-1 wt pct Al_2O_3 nanocomposite exhibits little enhancement in yield strength. It is likely that more Al_2O_3 nanoparticles were pushed to grain boundary. It is also possibly due to the fact that less Mg element is available to nucleate the age-hardened Mg_2Si phase, which leads to less age hardening and little enhancement in yield strength of nanocomposites after heat treatment. The Mg elements in the matrix can be depleted from the primary α-Al matrix and react with the Al_2O_3 nanoparticles, forming the $MgAl_2O_4$ phase around Al_2O_3 nanoparticles.[25] Only a small amount of Mg is required to form the $MgAl_2O_4$ spinel around Al_2O_3 nanoparticles, as 3Mg (l) + 4Al_2O_3 (s) → 3$MgAl_2O_4$ (s) + 2Al (l). During T6 solution treatment and subsequent aging, energy is supplied to increase the reaction of Mg and Al_2O_3 nanoparticles, increasing the formation of the $MgAl_2O_4$ spinel and consuming some/all of the Mg, limiting its yield strength enhancement. SEM photograph and EDS spectral mapping of T6 heat-treated Al-7Si-0.3Mg-0.5Cu-1 wt pct Al_2O_3 nanocomposite are shown in Figure 6. The result of EDS spectral mapping on the T6 heat-treated Al-7Si-0.3Mg-0.5Cu-1 wt pct Al_2O_3 nanocomposite exhibits that high amounts of Mg and O, as well as Al, are present, supporting the presence of the $MgAl_2O_4$ phase. STEM photograph with EDS analysis and ED comparison also reveal the presence of $MgAl_2O_4$ spinel phases in the matrix (Figure 7). Fine $MgAl_2O_4$ particles (marked by black arrows) of polyhedral morphology are exhibited along with the Al_2O_3 nanoparticle microclusters in the matrix. The EDS analysis shows elements O, Mg, and Al peaks, and the corresponding ED pattern is identified as $MgAl_2O_4$ spinel crystal.

IV. CONCLUSIONS

As-cast Al-7Si-0.3Mg alloys with various weight percentages of Cu and their nanocomposites with 1 wt
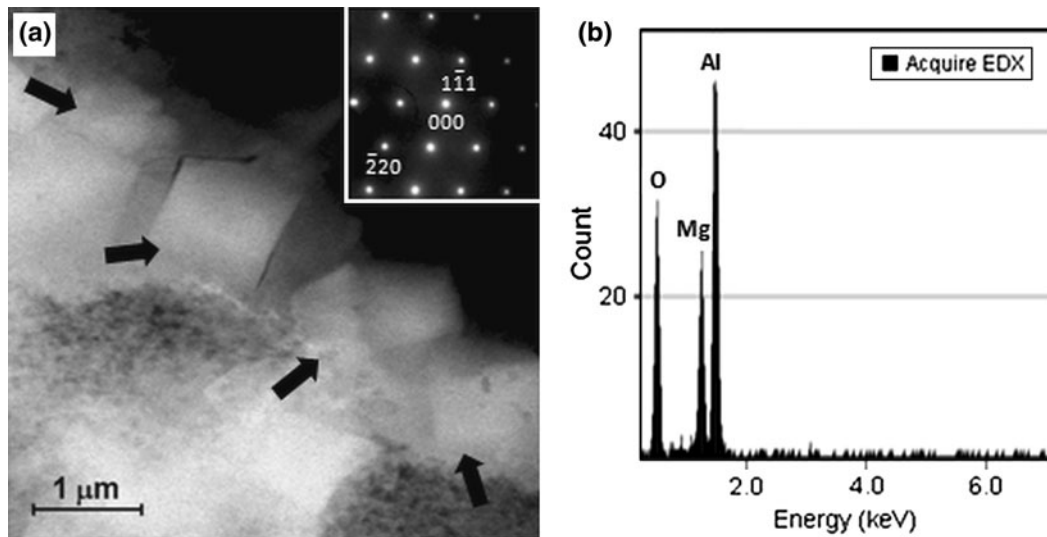
Fig. 7—(*a*) TEM photograph and electron diffraction pattern of MgAl$_2$O$_4$ spinel (indicated by arrows) in T6 heat-treated Al-7Si-0.3Mg-0.5Cu-1 pct Al$_2$O$_3$ nanocomposite. (*b*) EDS spectrum.

pct Al$_2$O$_3$ nanoparticles were fabricated to investigate the combined effect of Cu and Al$_2$O$_3$ nanoparticles on the mechanical properties and microstructures. Mechanical testing of those alloys suggests that 0.5 wt pct Cu would be a suitable weight of Cu to be added with Al$_2$O$_3$ nanoparticles in order to develop a high performance light alloy with higher strength and ductility. The enhancement of ductility (163 pct) and strength (13 pct in yield, 33 pct in tensile) is attributed to refinement of primary α-Al and modification of eutectic Si and θ-CuAl$_2$ phases. It was found that γ-Al$_2$O$_3$ nanoparticles could be a suitable nucleant of primary Al and eutectic Si phases in the Al-7Si-0.3Mg-0.5Cu alloy.

Pure Al-7Si-0.3Mg-0.5Cu alloy and its 1 wt pct Al$_2$O$_3$ nanocomposites were heat treated, under T6 condition, and their mechanical properties were tested. It was shown that the combination of 0.5 pct Cu and 1 pct Al$_2$O$_3$ nanoparticles results in a significant increase in ultimate tensile strength (22 pct). It is noticed that the ductility is improved from 1.7 to 10.4 pct (increased by 512 pct). The significant enhancement of properties is attributed to the decrease of porosity (from 2.1 to 0.5 pct) and modification of eutectic Si phases due to the addition of Al$_2$O$_3$ nanoparticles. The enhancement of yield strength in T6 heat-treated Al-7Si-0.3Mg-0.5Cu-1 wt pct Al$_2$O$_3$ nanocomposite was limited by the reaction between Mg and Al$_2$O$_3$ nanoparticles during the heat treating process.

REFERENCES

1. L. Hengcheng, S. Yu, and S. Guoxiong: *Mater. Sci. Eng. A*, 2003, vol. 358, pp. 164–70.
2. M.A. Gaffar, A. Gaber, M.S. Mostafa, and E.F. Abo Zeid: *Mater. Sci. Eng. A*, 2007, vol. 465, pp. 274–82.
3. J.E. Gruzieski and B.M. Closset: *The Treatment of Liquid Aluminum-Silicon Alloys*, American Society of Foundary, Des Plaines, IL, 1990, pp. 13–15.
4. G. Ran, J.E. Zhou, and Q.G. Wang: *J. Mater. Process. Technol.*, 2008, vol. 207, pp. 46–52.
5. J. Man, L. Jing, and S.G. Jie: *J. Alloys Compd.*, 2007, vol. 437, pp. 146–50.
6. M.A. Moustafa, F.H. Samuel, H.W. Dotty, and S. Valtierra: *Int. J. Cast Met. Res.*, 2002, vol. 14, pp. 235–53.
7. C.H. Caceres, M.B. Djurdjevic, T.J. Stockwell, and J.H. Sokolowski: *Scripta Mater.*, 1999, vol. 40, pp. 631–37.
8. K. Akio, O. Atsushi, K. Toshiro, and T. Hiroyuki: *J. Jpn. Inst. Light Met.*, 1999, vol. 49, pp. 149–54.
9. A. Mazahery, H. Abdizadeh, and H.R. Baharvandi: *Mater. Sci. Eng. A*, 2009, vol. 518, pp. 61–64.
10. Y. Yang, J. Lan, and X. Li: *Mater. Sci. Eng. A*, 2004, vol. 380, pp. 378–83.
11. G. Cao, H. Konishi, and X. Li: *Mater. Sci. Eng. A*, 2008, vol. 486, pp. 357–62.
12. H. Choi, N. Alba-Baena, S. Nimityongskul, M. Jones, T. Wood, M. Sahoo, R. Lakes, S. Kou, and X. Li: *J. Mater. Sci.*, 2011, vol. 46, pp. 2991–97.
13. K.S. Suslick and G.J. Price: *Annu. Rev. Mater. Sci.*, 1999, vol. 29, pp. 295–326.
14. D.Y. Ying and D.L. Zhang: *Mater. Sci. Eng. A*, 2000, vol. 286, pp. 152–56.
15. M. Kok: *J. Mater. Process. Technol.*, 2005, vol. 161, pp. 381–87.
16. M.P. De Cicco, L. Turng, X. Li, and J.H. Perepezko: *Metall. Mater. Trans. A*, 2011, vol. 42A, pp. 2323–30.
17. G.A. Edwards, G.K. Sigworth, C.H. Caceres, D. StJohn, and J. Barressi: *AFS Trans.*, 1997, vol. 105, pp. 809–18.
18. S. Ikeno, K. Matsuda, K. Nakajima, S. Rengakuji, and Y. Uetani: *J. Jpn. Inst. Light Met.*, 1998, vol. 48, pp. 207–11.
19. K. Matsuda, S. Ikeno, Y. Uetani, and T. Sato: *Metall. Mater. Trans. A*, 2001, vol. 32A, pp. 1293–99.
20. W.F. Li, X.L. Ma, W.S. Zhang, W. Zhang, Y. Li, and Z.D. Zhang: *Phys. Status Solidi A*, 2006, vol. 203, pp. 294–99.
21. D. Roundy, C.R. Krenn, M.L. Cohen, and J.W. Morris, Jr.: *Phys. Rev. Lett.*, 1999, vol. 82, pp. 2713–16.
22. S. Wu and H. Nakae: *J. Mater. Sci. Lett.*, 1999, vol. 18, pp. 321–23.
23. S. Hisashi, K. Motohiro, and I. Goroh: *J. Jpn. Inst. Light Met.*, 1980, vol. 30, pp. 609–16.
24. C.D. Lee: *Mater. Sci. Eng. A*, 2008, vol. 488, pp. 296–302.
25. A. Daoud and W. Reif: *J. Mater. Process. Technol.*, 2002, vol. 123, pp. 313–18.